Study of (He^3,d) and (He^3,t) Reactions in Light Nuclei at 25 Mev*

H. E. Wegner and W. S. Hall
Los Alamos Scientific Laboratory, University of California, Los Alamos, New Mexico
(Received April 28, 1960)

Angular distributions for the $Be^9(He^3,d)B^{10}$, $Be^9(He^3,t)B^9$, $C^{12}(He^3,d)N^{13}$, and $Ca^{40}(He^3,d)Sc^{41}$ reactions were measured at 25 Mev and also at 21 Mev for the carbon reaction. It was found that the angular distributions were strongly peaked forward, exhibited diffraction-like structure, and were asymmetric about 90°. The minimal positions of the angular distributions could be fitted with spherical Bessel functions of the appropriate order l, the angular momentum transfer of the ingoing proton. This analysis resulted in the same interaction radius for various levels in each of these reactions. The best-fit interaction radius for each case was 6.17, 5.91, 6.23, and 7.29 fermis, respectively. The Butler stripping theory was also fitted to the angular distributions; however, the average decrease of the angular distributions did not agree with the predicted decrease except in one case. The reactions exhibited the general characteristics of a direct process and could be predicted qualitatively with the simple form of direct interaction theories. The experimental equipment and the method of data analysis, using computer codes, is described. The ground-state Q values were measured for the $Ca^{40}(He^3,d)Sc^{41}$, $Ca^{40}(d,n)Sc^{41}$, and $O^{16}(He^3,d)F^{17}$ reactions. Q values for levels excited by the $Ca^{40}(He^3,d)Sc^{41}$ reaction were also measured.

I. INTRODUCTION

In recent years many experiments have been made with accelerated He^3 ions, primarily using Van de Graaff electrostatic accelerators. With these machines the energy has been limited to 6 or 7 Mev at the most, and, in general, the energy is too low to allow a study of the (He^3,d) and (He^3,t) reactions except in special cases. The recent installation of a He^3 recirculation system[1] at the Los Alamos variable-energy cyclotron has made avaliable He^3 ions in an energy range of 11 to 25 Mev and allows a study of the previously mentioned reactions in most of the light and medium-weight nuclei.

Because of the relatively low binding energy of both the input and reaction particles in the (He^3,d) and (He^3,t) reactions, a direct interaction would be expected at cyclotron energies. In general, it was observed that all of the angular distributions studied exhibited diffraction-like structure, were strongly peaked forward, and were asymmetric about 90°. These characteristics are those of a direct interaction and in many respects resemble a stripping process.

The (He^3,d) and (He^3,t) reactions are equivalent to the (d,n) and (p,n) reactions, respectively, in terms of the initial and final nuclides. The charged reaction products simplify the detection problem and consequently the study of these reaction nuclei. It is interesting to compare the (He^3,d) to the (d,n) reaction and the (He^3,t) to the (p,n) reaction in terms of the interaction mechanism. Those reactions leading to ground and low excited states can be a complex mixture of compound nucleus and various direct processes, and there is considerable experimental difficulty in separating these various reaction mechanisms.

The (He^3,t) reaction involves complex particles with relatively small mean free paths in nuclear material,[2] and the (p,n) process involves simple nucleons with relatively longer mean free paths, which enhances the probability of a direct knockout process from within the nucleus as well as from the surface. This effect implies that the (He^3,t) direct-exchange process is more exclusively a surface reaction than its (p,n) analog. A similar comparison for the (He^3,d) and (d,n) reaction cannot be made because the (d,n) process involves both a nucleon and complex particle. In the (He^3,t) case, such an experimental differentiation of surface effects may be of use in simplifying the theoretical analysis of these data. However, the relative role of compound nucleus vs direct interaction is not clear.

Angular distributions of the differential cross sections of various resolved levels, including the ground state, were measured for the $Be^9(He^3,t)B^9$, $Be^9(He^3,d)B^{10}$, $C^{12}(He^3,d)N^{13}$, and $Ca^{40}(He^3,d)Sc^{41}$ reactions. Various observed experimental correlations between the angular distributions and the known spins and parities of the levels of B^{10} and N^{13} were employed in the study of the reaction mechanism. These correlations were also used for predicting the spins and parities of the unknown levels of Sc^{41}. The highly negative reaction Q values of the $C^{12}(He^3,t)N^{12}$ and $Ca^{40}(He^3,t)Sc^{40}$ reactions, -17.5 and -14.0 Mev, respectively, apparently result in an extremely low cross section relative to other possible reactions. Tritons were not observed for these reactions.

II. EXPERIMENTAL ARRANGEMENT

Detector in Mass Separation

The detector used for this work consisted of a NaI(Tl) scintillation crystal for the detection of particle energy and a flow-type parallel plate ion chamber for the measurement of ΔE. Figure 1 shows the basic layout of the component parts. The guard ring on the center electrode was designed to correct the field distortion of the

* Work done under the auspices of the U. S. Atomic Energy Commission.
[1] H. E. Wegner and W. S. Hall, Rev. Sci. Instr. **29**, 12 (1958).
[2] G. Igo and R. M. Thaler, Phys. Rev. **106**, 126 (1957).

cylindrical geometry in the counter as well as the distortion caused by the bulging of the front window. In order to eliminate the back window, the NaI(Tl) crystal and light pipe were common with the ion chamber and were operated in the gas at counter pressure. The counter gas was a mixture of 5% CO_2 and 95% A. The quartz window that allows the light from the scintillation crystal to enter the photomultiplier tube was aluminized on the edges so that none of the light could be absorbed by the sealing O ring in contact with the window. The ΔE and E system was operated in a pressure range of 50 to 150 psi. The front window was 0.00025-in. permalloy foil,[3] 0.25 in. in diameter. The ion chamber became saturated at around 1000 v and was operated at 1600 v. The resolution for a given energy particle agreed with the theoretical prediction within the error of the measurements.[4] The resolution of the sodium iodide crystal (full width at half maximum) varied from 2.5% to 3%, depending on the particle being studied and on other conditions of the experiment.

Since the pulses of the ion chamber were small (no gas multiplication), it was important to maximize the signal by minimizing the input capacitance. For this reason, the counter system support included the preamplifier for the ion chamber, thereby eliminating the major part of the lead-in capacitance. By minimizing the capacitance and noise of the input stage of the preamplifier, the noise broadening was reduced to 10%–12% of the observed resolution width.

The pressure in the ΔE counter was held constant to 0.5% with a Cartesian manostat[5] on the outlet of the counter flow system. The temperature of the counter was maintained by water-cooling lines in the preamplifier chassis which eliminated possible vibration difficulties in the high-gain ΔE preamplifier input circuit that would be introduced by air cooling. In practice, it was found that the ΔE counter was stable over periods of weeks.

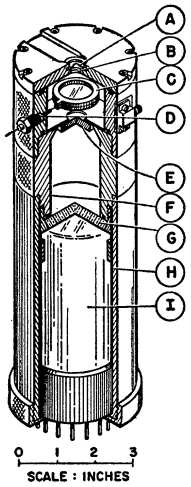

FIG. 1. dE/dx and E detector. (A) Interchangeable gold aperture. (B) Front window of counter. (C) Guard ring for collector plate. (D) Teflon insulator bushing. (E) NaI(Tl) crystal. (F) MgO smoked surface of light pipe. (G) Quartz window. (H) Mu-metal shield. (I) Photomultiplier tube.

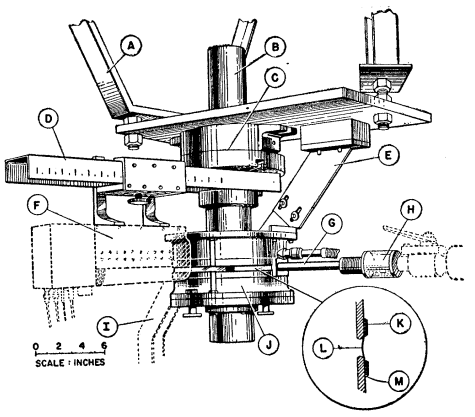

FIG. 2. Scattering chamber and detector support system. (A) System support frame. (B) Target position drive. (C) Rotary table. (D) Detector support boom. (E) Scattering chamber support arm. (F) Detector and preamplifier chassis. (G) Beam tube. (H) Collimator support. (I) Energy monitor support arm. (J) Scattering chamber. (K) Stainless steel compression band. (L) Mylar window. (M) Rubber pad.

Scattering Chamber

The scattering chamber, shown in Fig. 2, featured a thin continuous window and was basically similar to others reported in the literature[6] except for a simplification in the mechanical design. The chamber was 10 in. in diameter and did not require precision machining. It was coupled by a bellows to the cyclotron beam pipe so that the scattering geometry was not disturbed by scattering-chamber alignment. The rotating and sliding seal between the scattering chamber and the target support was arranged so that slight misalignments could be tolerated. In practice, the chamber was set concentric with the axis of rotation to approximately $\frac{1}{32}$ in. This accuracy was sufficient in terms of possible perturbations on the scattering geometry (for example, slight air-path length changes between chamber and counter window as the counter is rotated about the scattering chamber). Vacuum lock facilities were available at the base of the chamber. A small Faraday cup was provided inside the chamber and shielded by a set of permanent magnets as well as the usual electrostatic guard rings.

The scattering geometry is completely determined by a precision rotary table[7] on which the counter support boom and target holder are mounted as shown in Fig. 2. The target frame, which can be raised or lowered remotely, was supported through the axial bore in the table, so that the axis of rotation of the table passed through the plane of the target foils. Initially, the beam

[3] The Arnold Engineering Company, Marengo, Illinois.
[4] T. E. Cranshaw, *Progress in Nuclear Physics*, edited by O. R. Frish (Academic Press, Inc., New York, 1952), Vol. 2.
[5] Manostat No. 8, The Emil Greiner Company, New York, New York.
[6] M. K. Brussel and J. H. Williams, Phys. Rev. **106**, 286 (1957).
[7] Model BH9, The Troyke Manufacturing Company, Cincinnati 9, Ohio.

pipe was aligned with the rotary table so that the axis of the beam intersected and was perpendicular to the axis of rotation of the table. This adjustment completely determined the scattering geometry of the system, providing the counter was aligned with the intersection. The scattering chamber was then placed around the aligned system to form the vacuum envelope. The final aperture in the beam collimating system was 0.125 in. in diameter, and the size of the Faraday cup was such that it could subtend three mean square scattering angles from the thickest targets used.

The counter was usually operated in a position such that the extreme front of the counter cleared the window clamping bands by $\frac{1}{16}$ in., minimizing the air path in the window-to-window distance. The entire angular range could be covered by remote control with the counter in this position, except for the region of extreme back angles. In this region it was necessary to use a special counter vacuum extension which allowed the counter to be backed off far enough from the scattering chamber to clear the beam pipe and associated apparatus.

The scattering chamber window was 0.00025-in. Mylar and was continuous over the scattering-angle range of 5° left to 175° right and from 25° to 90° left, which allowed a right-left 0° determination. The window was cemented to the scattering chamber with Teflon cement[8] and was then clamped in place with steel bands padded with $\frac{1}{32}$-in. rubber, as shown in the inset of Fig. 2. Since the cement does not completely harden when used in this fashion, the compression bands must be supported vertically in several places to prevent the window tension from sliding the support bands together. The window was routinely changed between experiments (involving 50 to 100 hours of beam time). It was found that excessive bombardment of the window by scattered particles resulted in failure at the forward angles, probably due to radiation damage. The support boom was driven by a variable-speed transmission[9] which allows a counter boom motion smoothly adjustable up to a maximum speed of 10° per second. The transmission control and angle readout register were remoted with Selsyn transmitters.

Energy Monitor

A gold scattering foil was mounted at an angle of 45° to the beam direction inside the Faraday cup. A small hole in the bottom of the cup allowed beam particles scattered from the gold foil to pass into an energy monitor outside the scattering chamber. These scattered particles were decreased in energy by an aluminum absorber foil until the observed pulse height in a CsI(Tl) crystal was comparable to the pulse height observed from a plutonium alpha source which could be substituted remotely. This pulse height was monitored continuously during the experiment with a pulse-height reader,[10] allowing the energy of the cyclotron to be observed and reproduced. The energy errors quoted throughout the paper represent the range over which the energy was allowed to drift during the measurement.

Mass Selection System

The mass of the detected particles was selected by a ΔE and E system of measurement described by Stokes, Northrup, and Boyer.[11] The ΔE and E pulses were multiplied, resulting in a product proportional to mZ^2. The multiplier[12,13] allows the addition of two correcting factors in the multiplication. These factors partially correct for the thickness of the ΔE counter and the logarithmic term in the equation for ΔE. The multiplication performed was $(E+E_0+k\Delta E)\Delta E$ rather than $E\Delta E$ alone. By proper selection of k and E_0, an optimum mass separation could be obtained for any energy distribution over a wide range of energy. The mass spectrum observed for the (He^3,p), (He^3,d), and (He^3,t) reactions with Be^9 is shown in Fig. 3. In general, the mass spectra at other angles are similar to Fig. 3, except for the extreme forward angles where relative mass intensities may differ by orders of magnitude. The criterion for good mass separation is simply the peak-to-valley ratio between various mass peaks, and this ratio was optimized by k and E_0 adjustments.

In practice, an electronic gate was adjusted so that only multiplied pulses in the various mass-peak regions, as indicated in the figure, gate a multichannel analyzer. These gate settings then allowed the multichannel an-

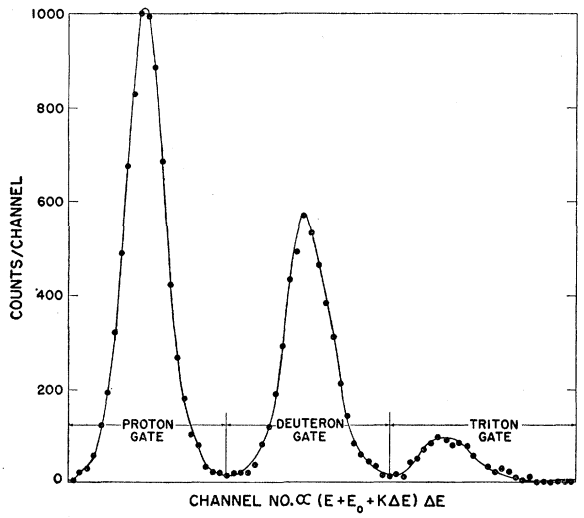

FIG. 3. Multiplier output at 20° for 24.37±0.15-Mev He^3 ions on Be^9. The positions of various gate settings are shown for separation of a given mass group from the mass spectrum.

[8] Teflon adhesive, Gilbreth Company, Philadelphia, Pennsylvania.

[9] Palley Supply Company, Los Angeles 58, California.

[10] J. A. Northrop and R. H. Stokes, Rev. Sci. Instr. **29**, 4 (1958).

[11] R. H. Stokes, J. A. Northrop, and K. Boyer, Rev. Sci. Instr. **29**, 1 (1958).

[12] William L. Briscoe, Rev. Sci. Instr. **29**, 5 (1958).

[13] R. H. Stokes, Rev. Sci. Instr. (to be published).

alyzer to display an energy spectrum of a particular mass particle. Since the mass separation was not perfect, there was always a small amount of leakthrough from one mass region to another. However, the leakthrough contributions could easily be determined by changing the gate settings while holding all the other electronic and cyclotron conditions constant.

III. EXPERIMENTAL METHOD

The beryllium and calcium targets used in this work were prepared by evaporation methods, and the carbon target was prepared by spraying an alcohol suspension of colloidal graphite on glass and then vacuum-outgassing the resulting foils. The targets were all self-supporting and were approximately 1 mg/cm^2 in areal density.

Besides the Faraday cup for monitoring the beam current, a stationary counter was employed at 30° left to monitor the elastically-scattered He^3 particles from the target. By moving the target up and down under beam conditions and observing the differences between the monitor counter, mass selecting counter, and integrated beam current, it was determined that the targets varied in thickness between 8% and 12%. Since the areal density was determined by weighing, the absolute cross section scale for any curve can be in error by as much as 12%. The target was not moved vertically during the experiment and rotations were compensated for by the monitor counter. Hence, the relative cross section was as accurate as the statistics and background would allow. The relative cross-section error is indicated by flags on the data points, and in cases where there are no flags, the statistical and background errors are less than or equal to the size of the points.

The acceptance angle at the detector over most of the angular range of the experiment was $\approx 2°$. At forward angles an absorber was used in front of the detector to cut off the elastic He^3 particles so that they could not enter the ΔE counter because the large forward-angle Coulomb cross section for elastically-scattered He^3 ions overloads the ΔE counter and spoils the separation efficiency of the system. The multiple Coulomb scattering correction for the absorber foil was negligible in the E counter at the rear of the ion chamber. The absorber was removed as soon as the elastic cross section was comparable to the reaction cross section. An aperture of 4° acceptance was used in the back angles. Since reaction particles decrease in energy with increasing scattering angles in the lab system, it was necessary to reduce the counter gas pressure in the ΔE counter in the back angle region. The back angle energy cut off by the ΔE counter limited the angular range of the $Be^9(He^3,t)B^9$ data, but did not limit the (He^3,d) data of interest.

IV. METHOD OF ANALYSIS

The gated pulses corresponding to the spectrum of a given mass group were stored in a 100-channel analyzer.

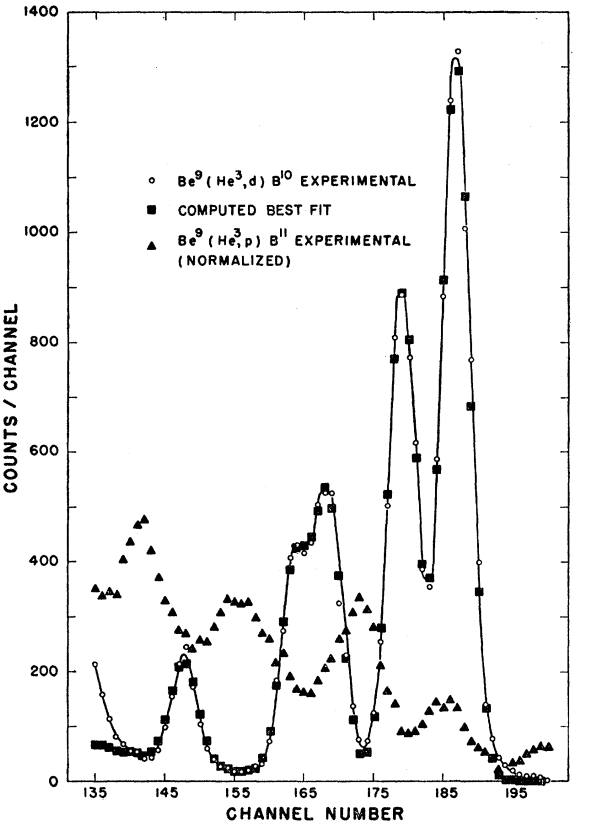

FIG. 4. A gated pulse-height spectrum for the $Be^9(He^3,d)B^{10}$ reaction at 17° superimposed with the "best fit" obtained by a Gaussian least-squares IBM-704 fitting code. He^3 energy = 24.37 ±0.15 Mev. Also shown are the experimental points for the $Be^9(He^3,p)B^{11}$ reaction obtained by changing multiplier gates (normalized to the deuteron gate data).

When sufficient data at a given angle had been accumulated, the 100 channels of information were printed, plotted, and punched on tape. A typical pulse-height spectrum for the $Be^9(He^3,d)B^{10}$ reaction is shown in Fig. 4. The data were relatively free of background, and the various peaks corresponding to the ground and excited states of B^{10} were analyzed for area to determine the relative cross section, which was then converted to absolute cross section from the known geometry of the system. The 21-Mev $C^{12}(He^3,d)N^{13}$ and 24-Mev $Be^9(He^3,t)B^9$ data were analyzed by adding up the number of counts under a given peak and subtracting the background, which was determined by inspection. The other data were machine-analyzed with an IBM-704 code.[14]

In practice, the punched tape was converted to IBM cards and the data analyzed by fitting a series of Gaussian curves superimposed on an exponential background. The code was given estimated peak positions, heights, widths, and the coordinates of two points that characterized the exponential background. The code

[14] R. H. Moore and R. K. Zeigler, Los Alamos Scientific Laboratory Report LA-2367 (unpublished).

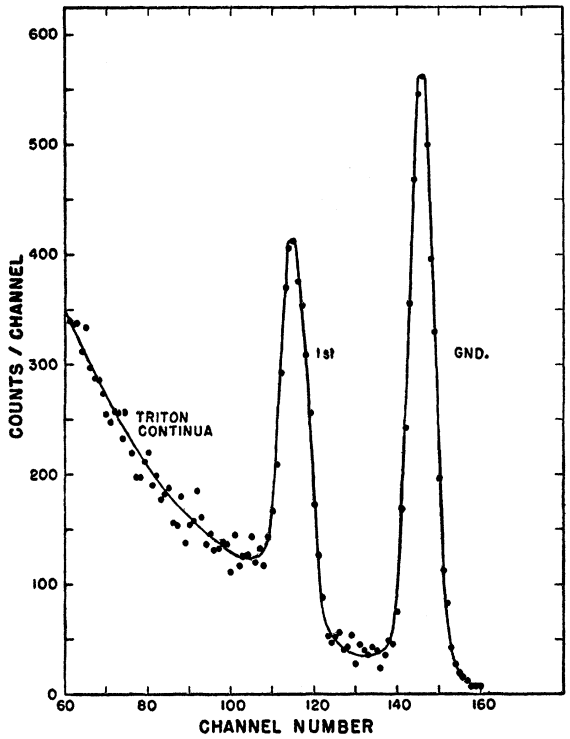

FIG. 5. A gated pulse-height spectrum for the $Be^9(He^3,t)B^9$ reaction at 68°. He^3 energy = 24.35±0.15 Mev.

adjusted the given parameters until a least-squares standard deviation was minimized. The areas of the best fit Gaussian curves with the background subtracted were then printed for each peak, along with the exact peak positions. The integrated beam current or monitor counter reading was automatically divided into the peak area, and the result was multiplied by a constant which converted the area to absolute cross section. These final output data, θ *vs* $d\sigma/d\Omega$, were also punched into cards as they were printed. The cards, in conjunction with another code, converted the laboratory data to the center-of-mass system. The center-of-mass data were also printed and punched, and these final punched cards were used to drive a standard plotting machine. All of the angular distributions shown in this paper were plotted by machine.

The quality of the fit determined by this code is indicated in Fig. 4. The response curve of the E detector is not exactly Gaussian and this difference is shown in the vicinity of channel 195 in Fig. 4. This small difference is completely consistent from peak to peak and does not affect the relative cross section. In general, this small error in absolute cross section was much less than the errors due to target nonuniformity.

Even in the cases where two peaks could not be completely resolved, the analysis was entirely consistent and allowed the unfolding of two or more unresolved peaks. Such analysis would be impractical by hand methods. In practice it was found that the best fit was achieved with approximately twelve iterations of the fitting parameters, and the computer time required was from three to five minutes per angle for a five-peak analysis.

V. RESULTS

$Be^9(He^3,t)B^9$—25 Mev (lab)

A typical mass spectrum illustrating the mass separation for this measurement is shown in Fig. 3. The gated spectrum obtained with the pulse-height analyzer is shown in Fig. 5. This spectrum shows tritons of energies corresponding to the ground state and higher to an excitation of approximately 5 Mev for B^9. These data are in agreement with a lower energy measurement by Spencer and Phillips[15] which was made with a magnetic spectrometer and indicated the possibility of one or two more levels. Such an indication with spectrometer resolution would be completely undetected with NaI(Tl) resolution. The spectrum is characterized by a ground and first excited state (2.326 Mev) superimposed on a continuum of tritons. Since B^9 is proton unstable, the probability of its formation in highly excited states is small, and with this particular reaction no other states were observed than the ground and first excited state. The triton continuum was investigated up to a B^9 excitation of 15 Mev at many different angles, and no other levels than those shown in Fig. 5 were observed. This result is in distinct contrast to the work reported at Washington by Lemonick, Cornwell, and Almquist[16] who investigated the $Li^7(He^3,n)B^9$ reaction. They reported four other levels besides those observed in this

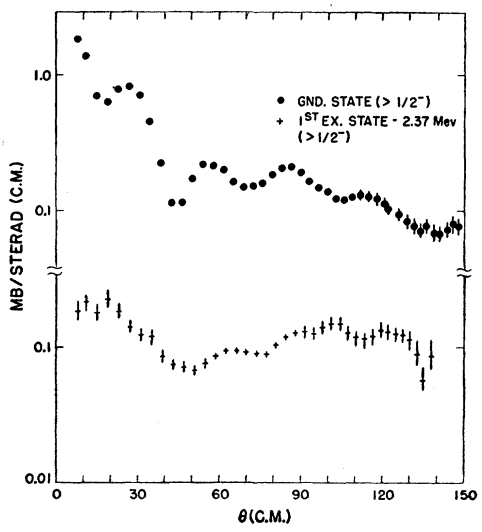

FIG. 6. Angular distributions of tritons from the $Be^9(He^3,t)B^9$ reaction. He^3 energy = 24.96±0.15 Mev.

[15] R. R. Spencer and G. C. Phillips, Bull. Am. Phys. Soc. 4, 95 (1959).

[16] A. Lemonick, R. G. Cornwall, and E. Almqvist, Bull. Am. Phys. Soc. 4, 219 (1959).

work. It is possible that these additional four levels are not excited by the $Be^9(He^3,t)B^9$ reaction.

The angular distributions of the ground and first excited states are shown in Fig. 6. The ground state is strongly peaked forward and shows a distinct diffraction-type structure, which carries through to the extreme back angles. The first excited state shows evidence of a slight diffraction-type structure, and the forward peaking is very modest. In general, the ground-state distribution strongly implies a direct interaction, whereas the first excited state implies more of a compound nucleus interaction.

$Be^9(He^3,d)B^{10}$—25 Mev (lab)

A typical spectrum for this reaction is shown in Fig. 4 and the mass spectrum is shown in Fig. 3. The angular distribution for the ground and first four excited states (0.72, 1.74, 2.15, and 3.58 Mev) are shown in Fig. 7. These distributions all show a strong forward peaking similar to the $Be^9(He^3,t)B^9$ data, and the oscillatory structure of the various angular distributions is in phase in the forward angles. The higher excited states up to a B^{10} excitation of 15 Mev were observed as a series of peaks comprised of many levels, but they are not shown. The angular distributions of these peaks are also not shown; however, they were peaked forward and showed no structure. The similarity in the forward angle part of the data from level to level, and in particular between the spin 0^+ and 3^+ levels, indicates that the reaction mechanism is relatively independent of level spin at these energies. The 0^+ level shows the most pronounced structure in the back angles, whereas the higher spin states show very little.

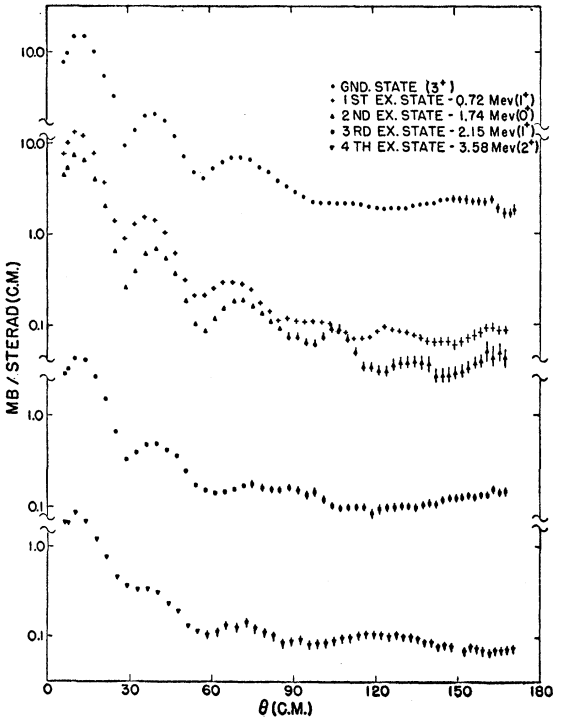

FIG. 7. Angular distributions of deuterons from the $Be^9(He^3,d)B^{10}$ reaction. He^3 energy = 24.98±0.15 Mev. The plots for the ground, third, and fourth excited states have been displaced vertically for clarity.

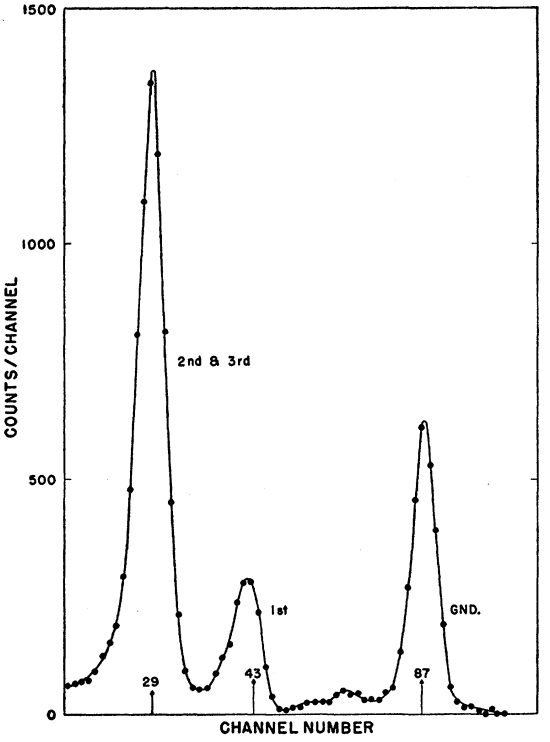

FIG. 8. A gated pulse-height spectrum for the $C^{12}(He^3,d)N^{13}$ reaction at 25°. He^3 energy = 21.64±0.2 Mev.

$C^{12}(He^3,d)N^{13}$—25 Mev and 21 Mev

Since the Q value for the $C^{12}(He^3,t)N^{12}$ reaction is −15 Mev, the tritons in this case were completely absorbed by the ΔE counter, and only protons and deuterons were separated with the detector system. The mass spectrum was similar to Fig. 3, except for the absence of the triton mass group. A typical gated spectrum for the $C^{12}(He^3,d)N^{13}$ reaction is shown in Fig. 8. The higher excited states (6.4, 6.9, and 7.4 Mev) are very weakly excited when compared to the ground state and are not shown. Since all of the excited states are subject to proton decay, a continuum of "three-body breakup" deuterons which partially obscured the higher levels was observed. The limited energy resolution of NaI(Tl) along with the deuteron background continuum resulted in poor reproducibility of the differential cross section. The angular distributions of these higher levels are not shown; however, they were strongly peaked forward with indications of oscillation.

The bad scatter of points in the angular distribution of the first excited state at 21.64 Mev (Fig. 9) and at 24.68 Mev (Fig. 10) was caused by the inability to

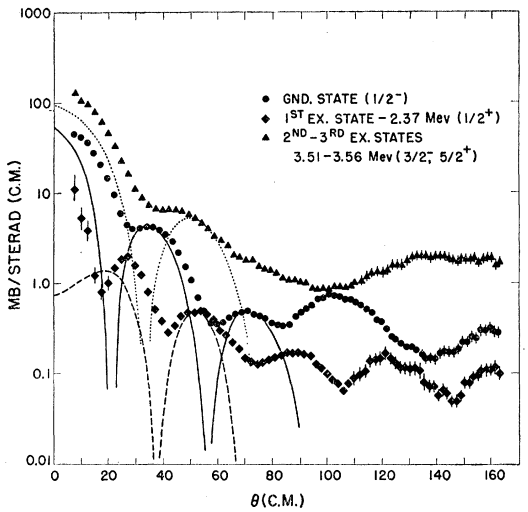

FIG. 9. Angular distributions of deuterons from the $C^{12}(He^3,d)N^{13}$ reaction. He^3 energy $=21.64\pm0.2$ Mev. The curves are the best fit with Butler stripping theory with an interaction radius of $(1.4A^{\frac{1}{3}}+1.3)$ fermis; solid curve, $l=1$; dashed curve, $l=0$; dotted curve, $l=2$.

separate the oxygen contribution from the carbon contribution at that particular region of angle. The small change in He^3 energy of 3 Mev modified the shape of the angular distribution slightly in the first excited state. The ground and unresolved doublet showed very little difference in structure with the change in energy.

The maxima and minima of the angular distributions of the ground and first excited states (2.37 Mev) were approximately out of phase throughout the entire angular distribution. The doublets were peaked forward similar to the ground and first excited states; however, the oscillatory structures were small compared to the first two levels.

$Ca^{40}(He^3,d)Sc^{41}$—24 Mev

The mass spectrum for this reaction was similar to that observed at 21 Mev with carbon. A gated deuteron spectrum for this reaction and the ground and several excited states are shown in Fig. 11. To simplify the discussion, the distinct peaks observed in Fig. 11 will be referred to as the ground state, first excited state, etc., although there are many other levels between these which are not excited by the (He^3,d) reaction. These states could be unresolved multiple levels representing single particle levels in the form of group structure.

Angular distributions of the differential cross sections for these levels are shown in Fig. 12. The distributions are strongly peaked forward and the first three levels show a modest diffraction-type oscillatory structure. The ground and first excited state show an out-of-phase characteristic throughout the entire angular range. The second excited state has an oscillatory behavior different from the ground and first excited state. The third and fourth excited states are monotonic and show no structure in the limited angular region investigated.

In the conversion from the laboratory system to the center-of-mass system, a Q value of -4.47 Mev was used for the reaction $Ca^{40}(He^3,d)Sc^{41}$. For the excited states of Sc^{41}, Q values of -6.16, -7.82, -9.57, and -10.48 Mev were used. These Q values were measured during the course of the experiment, and the method and details are described in the Appendix.

VI. DISCUSSION

Since the measured angular distributions in this work were predominantly for levels of light nuclei of known spins and parities, an analysis and comparison of their characteristics should indicate some of the general properties of the reaction mechanisms. The general characteristics of all the angular distributions were a strong forward peaking and an oscillatory behavior of the resolved single levels in the forward direction. These characteristics are indicative of a direct or surface-type interaction and may be understood qualitatively in terms of the general characteristics of simple direct interaction theories.[17]

The theories of direct interaction in their simplest form (Born approximation) result in a cross section proportional to some form factor F times a spherical Bessel function squared,[17]

$$d\sigma/d\Omega \approx F|j_l(qr)|^2,$$

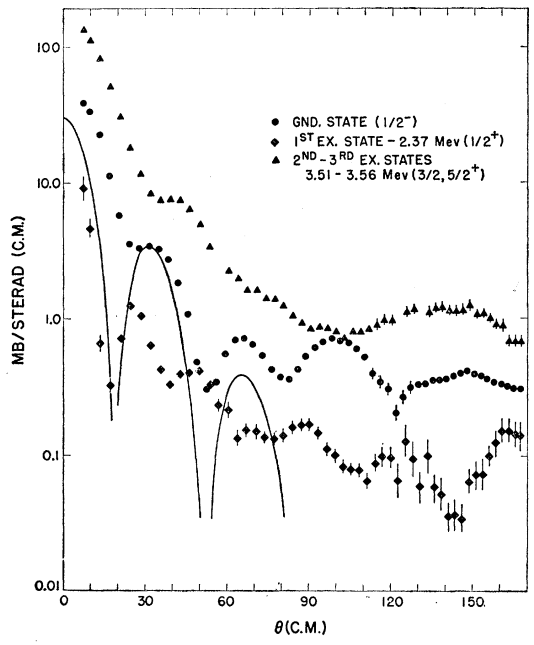

FIG. 10. Angular distributions of deuterons from the $C^{12}(He^3,d)N^{13}$ reaction. He^3 energy $=24.68\pm0.15$ Mev. The solid curve is a fit of the Butler stripping theory to the ground state with an interaction radius of $(1.4A^{\frac{1}{3}}+1.3)$ fermis and $l=1$.

[17] R. Huby, *Progress in Nuclear Physics*, edited by O. R. Frish (Academic Press, Inc., New York, 1953), p. 177.

where j_l=spherical Bessel function of argument qr and order l, q=momentum transfer, r=radius of the interaction, and l=number of units of angular momentum transferred, e.g., by the ingoing proton in the (He^3,d) reaction. The momentum transfer q is defined as

$$q=|\mathbf{p}_{\text{in}}-(M_i/M_f)\mathbf{p}_{\text{out}}|,$$

where $\mathbf{p}_{\text{in}}$=ingoing momentum of He^3 ion in the center-of-mass system, $\mathbf{p}_{\text{out}}$=outgoing momentum of the deuteron in the center-of-mass system, M_i=mass of the target nucleus, and M_f=mass of the recoil nucleus. The form factor can be very complicated, but in general depends monotonically on the momentum transfer and weakly on the initial and final state wave functions. The zeros of the Bessel functions result in a minimum cross section, regardless of the form factor which generally modifies the shape of the maxima and the average decrease of the distribution. Since the interaction radius determines the location of the zeros, it is of interest to fit the Bessel function zeros to the minima of the various angular distributions and observe the consistency between various sets of data. Even though the simple theories do not qualitatively fit the shape of the angular distributions, the minimal positions and corresponding zeros should have a close correspondence.

The selection rules require either an odd l value and an odd Bessel function or an even l value and an even Bessel function for a change or no change in parity, respectively, between the initial and final states. The only requirement on the magnitude of l is that the vector sum of the spins of the initial state plus the spin of the ingoing proton and chosen l value are equal to the spin of the final state. The most probable l is the lowest value that will satisfy the preceding conditions because the lower l values result in larger relative cross sections. Since the odd and even Bessel functions are out of phase with each other for a given interaction radius, angular distributions showing several maxima and minima in phase or out of phase should be of the same or different parity, respectively.

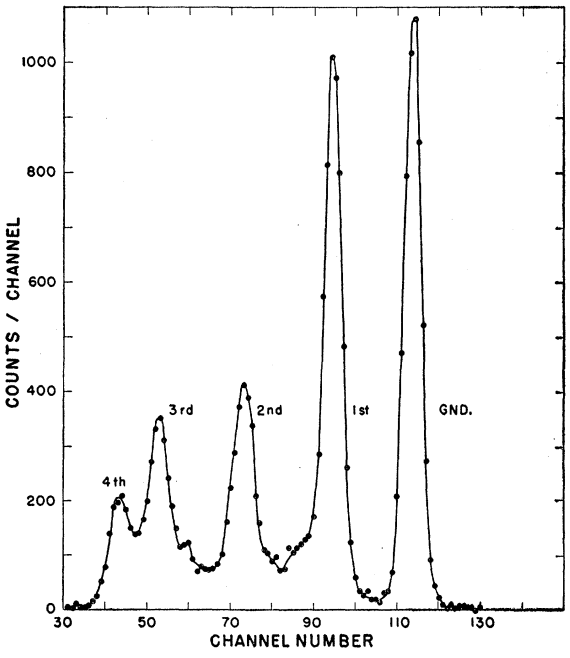

FIG. 11. A gated pulse-height spectrum for the Ca^{40}(He^3,d)Sc^{41} reaction at 41°. He^3 energy=23.65±0.15 Mev.

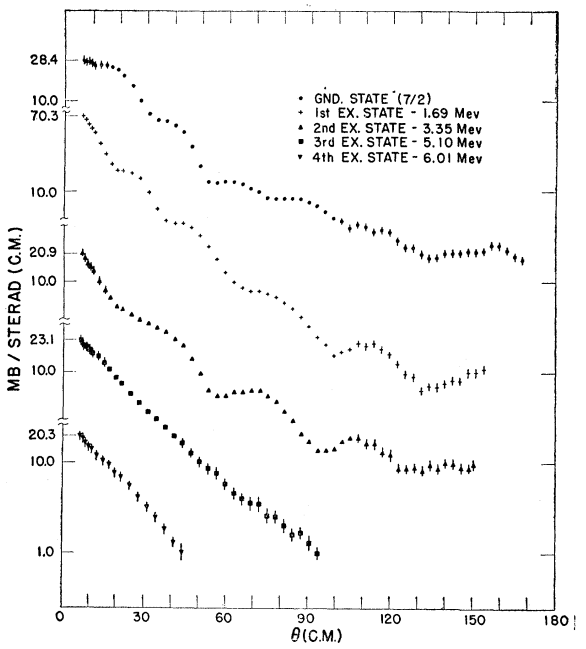

FIG. 12. Angular distributions of deuterons from the Ca^{40}(He^3,d)Sc^{41} reaction. He^3 energy=24.27±0.15 Mev. The plots for each level have been displaced vertically for clarity. The cross section of the first data point of each curve is indicated.

The second minimum, θ_{exp}, in each of the experimental angular distributions was normalized to the second zero, θ_1, of the appropriate spherical Bessel function by adjusting the interaction radius R_1. With this normalization, the angular position of the first, third, and fourth minima were predicted from the spherical Bessel function zeros and compared to the observed minimal positions. These comparisons are tabulated in Table I and show a reasonably consistent agreement, except for the first excited state of N^{13}. Since l=2 fits the distribution of the second and third excited states of N^{13} in the C^{12}(He^3,d)N^{13} reaction, the 5/2$^+$ level must be most strongly excited in accordance with shell model predictions.[18] The 3/2$^-$ level (l=1) is excited strongly enough to smooth out the distribution. Both sets of C^{12}(He^3,d)N^{13} data at 21 and 25 Mev were fitted with a single normalization at 21 Mev. The interaction radius, in general, appears to be quite consistent with interaction radii predicted from other similar measurements.

Rodberg, in a recent paper,[19] demonstrated how op-

[18] D. R. Inglis, Revs. Modern Phys. **25**, 390 (1953).
[19] L. S. Rodberg (in press).

TABLE I. A comparison of experimental angular positions of minima, θ_{exp}, with predictions based on spherical Bessel functions, θ_1 and θ_2.

Reaction	He^3 input energy (Mev)	Level	Angular momentum transfer	1st minimum (degrees)			2nd minimum (degrees)			3rd minimum (degrees)			4th minimum (degrees)			Interaction radii (fermis)
				θ_{exp}	θ_1	θ_2	θ_{exp}	θ_1	θ_2	θ_{exp}	θ_1	θ_2	θ_{exp}	θ_1	θ_2	R_1 and R_2
$C^{12}(He^3,d)N^{13}$	21	Ground	$l=1$	29.0	28.5	29.9	58.5	58.5[a]	58.5[a]	84.0	91.6	89.6	138	139	133	$R_1=6.23$
		1st	$l=0$	17.5	<0	15.2	42	45.1	45.8	74.5	78.2	75.5	106	120	112	$R_2=4.22$
		2nd, 3rd	$l=2$	39.0	39.0	41.0	70[c]	75.7	72.6	100[c]	119	107	[c]			
$C^{12}(He^3,d)N^{13}$	25	Ground	$l=1$	28.0	26.0	28.7	54.0	54.0	56.7	82.0	83.4	85.9	123	121	125	$R_1=6.23$
		1st	$l=0$	17.5	<0	14.3	39.0	41.4	44.0	77.0	71.0	72.4	110	106	106	$R_2=4.22$
		2nd, 3rd	$l=2$	37.0	35.0	39.3	69[c]	68.5	69.5	100[c]	105	102	[c]			
$Be^9(He^3,d)B^{10}$	25	Ground	$l=1$	27.5	30.5	30.0	56.0	57.2[b]	56.8	99.0	86.5	85.6	[c]			$R_1=6.17$
		1st	$l=1$	27.5	30.3	29.9	56.0	57.5[b]	56.8	86.0	87.3	86.1	114	127	125	$R_2=4.41$
		2nd	$l=1$	29.0	30.0	29.6	57.0	58.0[b]	57.0[a]	90.0	88.4	86.6	123	130	126	
		3rd	$l=1$	29.0	29.8	29.6	61.5	58.1[b]	57.1	[c]			[c]			
		4th	$l=1$	30.0	29.2	29.3	59.0	58.7[b]	57.4	94.0	90.7	87.7	[c]			
$Be^9(He^3,t)B^9$	25	Ground	$l=0$	19.0	21.8	21.8	44.5	44.5[a]	44.5[a]	71.0	69.2	69.2	105	98.5	98.5	$R_1=5.91$
		1st	$l=0$	[c]			50[c]	45.9	45.2	[c]			[c]			$R_2=4.14$
$Ca^{40}(He^3,d)Sc^{41}$	25	Ground	$l=3$	32.0	32.4	33.5	54.0	54.0[a]	54.0[a]	76.0	75.6	74.8	105	100	98.4	$R_1=7.29$
		1st	$l=1$	19.0	11.5	17.0	39.0	36.7	37.8	69.0	57.7	57.3	100	79.7	78.0	$R_2=5.06$
			$l=2$		22.9	25.6		45.7	46.1		67.3	66.3		90.7	88.4	
		2nd		21.0[d]			58.0[d]			95.0[d]			130[d]			

[a] Minimal position chosen for the determination of the interaction radius.
[b] The average of these angles was used to determine an average interaction radius.
[c] These experimental minimal positions are either questionable or not observed.
[d] These experimental angles may be compared to predictions for $l=1$, 2 and 3 by comparison to the l values for the ground and first excited states.

tical model interaction radii could be predicted from the minimal positions in the elastic angular distributions without resorting to an optical model calculation. An extension of his method to reaction scattering[20] is accomplished by a change in the ingoing momentum $\mathbf{p}_{in}$. Instead of the usual $\mathbf{p}_{in}$ used previously in the definition of momentum transfer, an adjusted ingoing momentum $\mathbf{p}_{in}'$ is defined

$$|\mathbf{p}_{in}'|=[(E-V)2m]^{\frac{1}{2}},$$

where E= the kinetic energy in the center-of-mass system, m= mass of the incoming particle, and V= effective potential well depth. In the case of the He^3 data in this paper, $V=25$ Mev results in an interaction radius R_2 which is approximately that predicted by high-energy electron scattering.[21] The corresponding $\mathbf{p}_{in}'$ was used in calculating q and the associated Bessel-function minimal positions θ_2. These predicted minima are also listed in Table I, and it is noted that the minimal positions are only slightly changed except for the first excited state of N^{13} which could not be fitted with the simple expression for q. This level is now reasonably fitted. Since the well depth for He^3 is probably similar to that for alpha particles (≈ 50 Mev), the best fit for $V=25$ Mev could possibly be interpreted to mean that the interaction is occurring approximately halfway into the nuclear surface. The improved fit of a single distribution with little change in the others hardly justifies the modification. However, Rodberg finds that this method results in a more consistent radius for a wider variety of reactions.[20]

Only the ground state of Sc^{41} could be fitted by the spherical Bessel functions with a unique l, whereas the first and second excited states could be equally well fitted with different l values. The first excited state actually fits $l=2$ slightly better than $l=1$. The experimental minima of the second excited state may be compared to $l=1$, 2, and 3 by inspection, and it is clear that a reasonable fit is impossible. Coulomb effects undoubtedly distort the angular distribution to some degree and may account for the general smoothing of the distribution. Since the ground state distribution fits very well, it is unlikely that Coulomb effects are responsible for the difficulty in fitting the excited states. This difficulty could be due to either the possible multiple characteristics of the observed excited states or else a different effective interaction radius for each level. The ground state spin of $7/2^-$ is in agreement with these data; however, no definite spin or parity assignments can be made for the excited states.

Since the minimal fits are quite consistent, it would appear that a Butler-stripping-theory calculation would result in a more qualitative fit because the decrease with angle of the Bessel functions is much less than that observed. The usual Butler-stripping calculation for the (d,p) process involves the wave function of the deuteron and hence, in this case, involves the wave function of the He^3 nucleus. The usual approach is to approximate the He^3 wave function as a deuteron plus a bound proton in first-order approximation. J. E. Young of this Laboratory performed the calculation in the following way.

The cross sections for $X(He^3,d)Y$ are calculated in Born approximation with a model suggested by Thomas.[22] The residual nucleus is expanded over the complete set of states $X+p$, and the pickup amplitude (d,He^3), leaving X in its ground state, is computed. The usual arguments of detailed balance are then employed to obtain the direct cross section from its inverse. In this formalism, the proton separation energy η is a parameter that affects the general decrease of the angular dis-

[20] L. S. Rodberg (private communication).
[21] D. G. Ravenhall, Revs. Modern Phys. **30**, 430 (1958).
[22] R. G. Thomas, Phys. Rev. **100**, 25 (1955).

tribution (shape of the form factor) and is adjusted for best fit.

The results of this calculation are shown in Fig. 9 in comparison with the C^{12}(He,d)N^{13} data at 21.64 Mev. The separation energy and interaction radius were chosen for the best fit with the ground state (spin $1/2^-$, $l=1$); these same parameters were used to fit the excited states with appropriate changes in l and the reaction Q value. The amplitudes were arbitrarily normalized as shown. The ground state fit was very good except for the forward angles and regions near the minima. The form factor predicted the decrease with angle quite accurately corresponding to a proton separation energy η of 8 Mev. Actually, a change of ± 2 Mev in η only slightly modifies the decrease with angle.

The first excited state did not fit the forward angles even qualitatively since the first maximum and minimum were not predicted. The same difficulty is observed for the Bessel function (Table I). The second and third excited states compared moderately well; however, only one peak is shown, and it was difficult to ascertain the quality of the fit because of the difference in the forward angle.

The C^{12}(He^3,d)N^{13} reaction at 24.68 Mev was compared to Butler theory in a manner similar to that used for the 21-Mev data, as shown in Fig. 10. The same parameters were used except for a change in energy. It was observed that the experimental decrease is less rapid than that predicted. In order to bring the theoretical curve up to the experimental data of the second maximum, an unreasonable separation energy for the proton of more than 30 Mev would have to be assumed. The recent measurement by Priest *et al.*[23] of the C^{12}(He^3,d)N^{13} angular distribution for the ground state at 13.9 Mev was also fitted with these parameters, and again the theoretical prediction decreased much more rapidly with angle than the experimental data.

The other data in this paper were also compared with the predictions of Butler theory, and none of the other curves could be fitted with reasonable parameters. Since only one of the curves could be fitted, it would seem that this fit is fortuitous rather than physically significant. Apparently the simple assumptions in the Butler theory are inadequate to explain the (He^3,d) interaction. The difficulty with these theoretical comparisons demonstrates the importance of measuring more than a single level for a given interaction at different energies.

A distorted wave calculation by Henley[24] for the direct (α, nucleon) reaction predicts angular distributions similar to those observed for the Ca^{40}(He^3,d)Sc^{41} reaction. This calculation, as well as other recent work,[25] could be applied to these data by appropriate extensions of the calculations.

A recent theory by Glendenning[26] of direct-interaction inelastic scattering can be used to fit the Be^9(He^3,t)B^9 data. The two-nucleon force has a charge exchange part which can be used to transfer the charge of a proton in the projectile to a neutron in the target. This theory can be applied to the (He^3,t) reaction by assuming that this exchange part of the cross section is solely responsible for the (He^3,t) reaction. The resulting theoretical curve was quite different from the experimental data and is not shown. The conclusion is that the (He^3,t) exchange reaction is considerably more complicated than this theoretical model.

Another experimental correlation that has not been predicted, but which may bear on future theoretical work applied to these data, is a tendency for a decrease of the diffraction-like structure in the backward angles with increasing level spin of the final state in the Be^9 (He^3,d)B^{10} data. It is also interesting to note that the angular distribution of the ground state in the Be^9(He^3,t)B^9 reaction (no change in parity) is very similar to the angular distribution of the first excited state in the C^{12}(He^3,d)N^{13} reaction (no change of parity). The similarity may be fortuitous, or it may indicate that the reaction mechanism for both reactions is very similar.

ACKNOWLEDGMENTS

The authors gratefully acknowledge helpful discussions with J. E. Young, of the Los Alamos Scientific Laboratory, and L. S. Rodberg, a consultant to this Laboratory.

APPENDIX

The measured reaction Q value for the Ca^{40}(He^3,d)Sc^{41} reaction is in disagreement with currently accepted values[27] by 0.6 Mev, resulting in a revised mass for Sc^{41} of 40.982355 ± 0.000100 amu. Since this measurement is in disagreement with a previous Ca^{40}(d,n)Sc^{41} measurement[28] and also a $Sc^{41}\rightarrow\beta^+ + Ca^{41}$ beta-decay end-point measurement,[29] these measurements were reinvestigated.

The relative mass of Ca^{40} and Ca^{41} has been precisely determined by Bockelman and Buechner through the Ca^{40}(d,p)Ca^{41} reaction.[30] Since Sc^{41} undergoes beta decay to Ca^{41} and is produced from Ca^{40} by the Ca^{40}(d,n)Sc^{41} and Ca^{40}(He^3,d)Sc^{41} reactions, the ground state Q values for the (d,n) and (He^3,d) reactions were compared to the revised β^+ end point in terms of the Ca^{40} and Ca^{41} relative masses. This comparison resulted in agreement within experimental errors, confirming the revised mass of Sc^{41}.

[23] J. R. Priest, O. J. Tendam, and E. Bleuler, Bull. Am. Phys. Soc. **5**, 45 (1960), and private communication.
[24] E. M. Henley, Nuclear Phys. **13**, 317 (1959).
[25] S. T. Butler, N. Austern, and C. Pearson, Phys. Rev. **112**, 1227 (1958).
[26] Norman K. Glendenning, Phys. Rev. **114**, 1297 (1959), and private communication.
[27] V. J. Ashby and H. C. Catron, University of California Radiation Laboratory Report UCRL-5419, 1959 (unpublished).
[28] H. S. Plendl and F. E. Steigert, Phys. Rev. **116**, 1534 (1959).
[29] D. R. Elliot and L. D. P. King, Phys. Rev. **60**, 489 (1941).
[30] C. K. Bockelman and W. W. Buechner, Phys. Rev. **107**, 1366 (1957).

$Ca^{40}(He^3,d)Sc^{41}$ Reaction

The experimental arrangement and equipment are described in Sec. II. Briefly, 25-Mev He^3 ions bombarded carbon, beryllium, and calcium targets which were alternately placed in the scattering chamber. The (He^3,d) spectra for each of the reactions were then superimposed for calibration purposes. The energy in the laboratory system E_{lab} of the deuteron groups was calculated for each of the known Q values.[31] From these values of E_{lab}, a plot of E_{lab} vs channel number was made, which was a straight line over much of the region of interest. The channel number corresponding to each peak location was determined by the IBM-704 code described in Sec. IV. The E_{lab} corresponding to the energy levels of Sc^{41} was then determined from this calibration curve and converted back to the Q values for each of the unknown levels. Both calculations were done relativistically with a $Q \rightleftarrows E_{lab}$ conversion code. The measurement described was performed at 10°, 20°, 40°, and 80°. There was a different calibration curve at each angle, because as the angle increases, the deuteron groups from the lighter elements lose energy in the laboratory system faster than the deuteron groups from the $Ca^{40}(He^3,d)Sc^{41}$ reaction.

The results of these measurements were consistent at the various angles, which confirms their mass identification. Five peaks were observed with Q values of -4.47 ± 0.10, -6.16 ± 0.15, -7.82 ± 0.15, -9.57 ± 0.20, and -10.48 ± 0.20 Mev. These levels are shown graphically in Fig. 13. Because the previously reported Q value for this reaction is -3.87 Mev,[27] a change of 0.6 Mev in the mass of Sc^{41} is indicated, resulting in a revised mass of 40.982355 ± 0.000100 amu.

With the above mass correction applied to the proton elastic scattering work of Class *et al.*,[32] resonances observed at a Sc^{41} excitation energy of 3.96, 5.69, and 6.58 Mev correspond approximately to the levels with Q values of -7.82, -9.57, and -10.48 Mev for the $Ca^{40}(He^3,d)Sc^{41}$ reaction. Actually, 42 resonances were observed by Class *et al.*, and their widths γ were measured between 2.06- and 5.75-Mev excitation. The energy location of these levels is indicated in Fig. 13. The ratio γ_w of these widths to the Wigner limit was compared for levels of the same l (or j). A portion of this comparison[32] is shown in Fig. 13 and indicates that the three highest levels observed by the $Ca^{40}(He^3,d)Sc^{41}$ reaction occur at energies where single-particle levels would be expected.

$Ca^{40}(d,n)Sc^{41}$ Reaction

The reported Q value for the $Ca^{40}(d,n)Sc^{41}$ reaction[28] is in agreement with older data[29] and results in a mass of Sc^{41} in disagreement by 0.6 Mev with the previously mentioned measurements. An independent measurement of the $Ca^{40}(d,n)Sc^{41}$ reaction was made in collaboration with Jules S. Levin, using the Los Alamos pulsed-beam, neutron time-of-flight system.[33] Deuterons were accelerated to 4 Mev in the Los Alamos vertical electrostatic generator, and bombarded an evaporated calcium target on a gold backing. These measurements were made at 60°, 90°, 120°, and 150°. Four peaks were observed in addition to the gamma-ray peak. Two were due to the ground and first excited states from the $O^{16}(d,n)F^{17}$ reaction, and two from the ground and first excited states from the $Ca^{40}(d,n)Sc^{41}$ reaction. The peaks were identified by the manner in which their corresponding laboratory energy changed with angle. The known Q values[31] of the peaks from the oxygen reaction were then used to calibrate the time scale which determined the energy of the other two peaks corresponding to the ground and first excited states of Sc^{41}. The results were analyzed with the same $Q \rightleftarrows E_{lab}$ code used previously and were found to be consistent at each angle.

Preliminary results give a Q value of -1.32 ± 0.07 Mev for the reaction $Ca^{40}(d,n)Sc^{41}$ and a Q value of -2.85 ± 0.03 Mev for the first excited state. These data are in agreement with the Sc^{41} mass and first excited state energy measurements by the $Ca^{40}(He^3,d)Sc^{41}$ reaction, and are in disagreement with the $Ca^{40}(d,n)Sc^{41}$ work of Plendl and Steigert.[28] The small difference of 0.12 Mev in the mass of Sc^{41} between the (d,n) and (He^3,d) measurements is within errors, but could be real if unexpected unresolved levels near the ground state were excited more by one reaction than the other. A comparison of the previous work[28] and the present work is shown in Fig. 13.

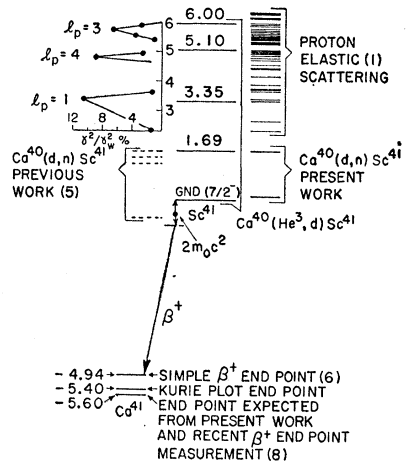

FIG. 13. Comparison of ground state and energy levels of Sc^{41} measured by different methods.

End-Point Measurement of Sc^{41} β^+ Decay

The currently accepted value for the mass of Sc^{41} is apparently based primarily on the 1941 β^+ spectrum

[31] F. Ajzenberg-Selove and T. Lauritsen, Nuclear Phys. **11**, 1 (1959).

[32] C. M. Class, R. H. Davis, and J. H. Johnson, Phys. Rev. Letters **3**, 41 (1959); and private communication.

[33] L. Cranberg and J. S. Levin, Phys. Rev. **103**, 343 (1956).

end-point measurement of Elliot and King.[29] The end point was obtained by simple extrapolation of the actual β^+ spectrum. In cooperation with B. J. Dropesky of this Laboratory, the fermi functions were computed for this particular isotope and energy range, and a Kurie plot of the 1941 data was made. Since the data were taken with a cloud chamber, the statistical accuracy was limited; however, a considerable portion of the spectrum resulted in a straight line with the end-point energy of 5.3±0.1 Mev rather than the 4.94 Mev reported. The predicted end point from the $Ca^{40}(He^3,d)Sc^{41}$ and $Ca^{40}(d,n)Sc^{41}$ reactions is 5.60 Mev. A discrepancy is still indicated, although the revised β^+ value is increased in the direction of the predicted end points. Preliminary results of a recent measurement of this β^+ spectrum by Class, Farmer, and Cramer at the Rice Institute[34] indicate the end point to be 5.65±0.10 Mev in approximate agreement with the predicted end point. These results are also indicated in Fig. 13.

$O^{16}(He^3,d)F^{17}$ Reaction

Since oxygen was present as a contaminant in the targets used, it was possible to measure the Q value for the $O^{16}(He^3,d)F^{17}$ reaction. The measured Q value of -4.90 ± 0.09 Mev is in agreement with the calculated value[28] and has not been previously reported.[27]

[34] J. G. Cramer, B. J. Farmer, and C. M. Class (to be published); and private communication.

PHYSICAL REVIEW VOLUME 119, NUMBER 5 SEPTEMBER 1, 1960

Angular Correlation of Annihilation Radiation in Sulfur and Its Compounds*

P. COLOMBINO, I. DEGREGORI, L. MAYRONE, AND L. TROSSI
Instituto de Fisica, Universita' di Torino, Torino, Italia
AND
S. DEBENEDETTI
Carnegie Institute of Technology, Pittsburgh, Pennsylvania

(Received April 11, 1960)

The angular correlation of annihilation radiation in elemental sulfur and in several sulfur compounds was found to be practically the same in all samples studied. The observed correlation is similar to that observed with chlorine salts; a similarity that, in some cases at least, may be correlated to the similarity of the ions Cl^- and S^{--}.

THE angular correlation between the γ rays of positron annihilation has been measured in samples of sulfur in different allotropic states, in chemical compounds of sulfur, and for comparison in some salts not containing this element.

The elemental sulfur was studied in the rhombic,

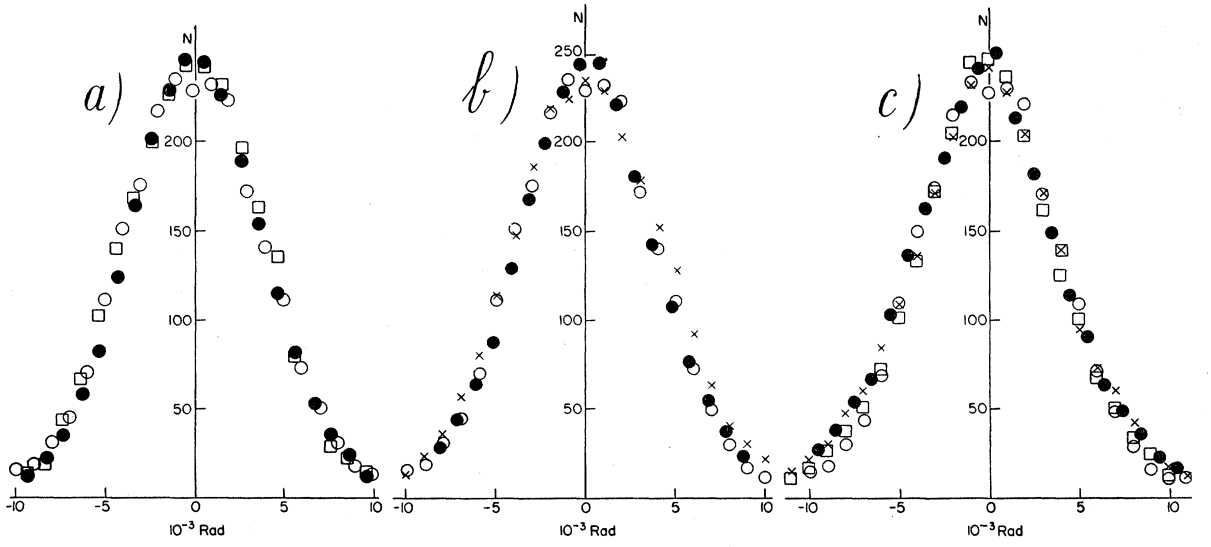

FIG. 1. The angular correlation between γ rays from position annihilation: (a) ○ *S* rhombic (20°C); ● *S* plastic (20°C); □ *S* monoclinic (105°C), (b) ○ *S* rhombic; ● Na_2S; × FeS, (c) ○ *S* rhombic; ● Cs_2SO_4; × Li_2SO_4; □ Na_2SO_4. The curves are normalized to the same area.

* At the Carnegie Institute of Technology positron research is supported by a National Science Foundation grant.